# The Application of Sensorless-Based Torque **Estimation Technique in Industrial** Collaborative Robots

Isak Martin Simbolon\* and Yun-Yu Yang

Abstract—Traditional industrial robots often require separate work areas and safety equipment to avoid human collisions, restricting their use in smaller or densely populated environments. Most commercially sold robots use position control, and adding force control requires a force sensor, which can be costly. This research introduces a power-assisted collision detection strategy directly implemented on the controller, eliminating the need for an external force sensor. The mathematical model calculation module estimates the robot's friction, and inertial force, while the collaborative function algorithm refines the robot arm's flexible function. The driver's torque limit mechanism is essential for safe human-robot collaboration. By controlling the joint module's torsion in the mechanical arm, the robot can prevent potential injuries from human contact. If contact occurs, the robot can be easily pushed away, safeguarding personnel. Once any issues are addressed, the robot resumes its original work target, enhancing the overall efficiency of the collaborative process.

Index Terms—force control, industrial robot, sensorless control

#### I. INTRODUCTION

HE interaction and collaboration between humans and I robots in a physical setting have become significant area of interest and focus in robotics research. In service-related applications and potentially in upcoming industrial applications, tasks that involve humans and robots working together in the same workspace will require the development of reliable and secure robot designs and control systems [1].

There are several different types of control schemes that can be used in human-robot interaction, depending on the specific application and the requirements of the user. Some common examples include teleoperation [2], gesture-based control [3], and voice-based control [4]. The choice of control scheme depends on a range of factors, including the specific application, the level of human involvement required, and the capabilities of the robot.

Compliance control in robotics refers to a control method that allows a robot to adjust its movements and forces in response to external forces. Compliance control is often used in applications where the robot needs to operate safely and interactively with its environment, such as in human-robot collaboration for object carrying [5]. Gorjup et al. [6] combine CAD-based component localization, compliance control, and a multi-modal gripper to enable robust and efficient programming of complex tasks for assembly robots.

Isak Martin Simbolon is with Precision Machinery Research & Development Taichung Center, City, Taiwan. e11138@mail.pmc.org.tw).

Yun-Yu Yang is with Precision Machinery Research & Development Center, Taichung City, Taiwan. (e-mail: e10528@mail.pmc.org.tw).

Dong et al. [7] proposed an active disturbance rejection velocity feedback loop within the outer PD torque loop in a compliance control scheme. By doing so, the joint torque servo controller they proposed can accurately follow the desired signals while also actively estimating and eliminating any disturbances, even without explicitly modeling the plant or perturbations. Mou et al. [8] proposed a sliding mode control technique with an active disturbance rejection control (ADRC) technique to achieve a good performance against external disturbances when the robot is required to do a wide range of motion.

The design of collaborative robots often includes safety features, especially by adding a way to detect forces. In [9], a force control strategy by adding a compliant sensor with a position control scheme is examined. This method enables quick responses to unanticipated forces resulting from a collision between the robot's tool and an immovable, rigid object.

Another method is by installing a joint torque sensor on the robot [10]. Zhang et al. [11] improve the joint torque sensor by adding a disturbance elimination method in a modular joint, which results in better accuracy even with electromagnetic noise. Nonetheless, this method uses an additional sensor raises the expenses associated with production, which poses a challenge in implementing robot arms in low-priced service contexts.

In this paper, we propose a safety collision detection strategy based on the torque limit mechanism and the torque estimation that does not rely on an additional force sensor. This torque estimation is obtained by analyzing the system model in motion, thus improving the cost efficiency while also developing a safety mechanism. Once any issues are addressed, the robot resumes its original work target, enhancing the overall efficiency of the collaborative process.

The rest of the paper is organized as follows: Section II first reviews the SCARA robot that is used for the experiment. Section III explains the method for the control scheme and also explains the robot dynamics. Section IV describes the powerassisted collision detection strategy for various modes. Finally, experiments are presented, and a conclusion is given.

# II. THE URDF MODEL OF THE SCARA ROBOT

The target application of this research is deployed in SCARA Robot for the second and the third joint of the robot, as shown in Fig. 1. The URDF model is usually used in ROS (Robot Operating System). This study borrows the design concept of URDF as a modeling tool for simulating the robotic arm. The traditional URDF model is only used to calculate the coordinates of each axis of the manipulator.

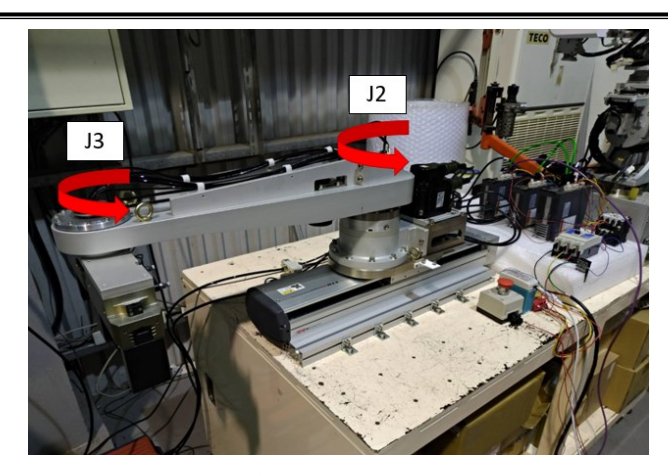


Fig. 1. SCARA Robot

Through the URDF model, the configuration and related parameters of the robot can be described, such as joint position, rotation axis, and center of mass position. In the definition of each joint, the reference point is consistent with the base of the previous joint.

The URDF parameters for the SCARA robot in this project are shown in Table 1 and visualized as shown in Fig. 2. Where X, Y, and Z are displacement of the joint to the previous joint base, and Rx, Ry, and Rz are the rotation axis that either 0 or 1, where 0 indicates the axis is a fixed axis, and 1 indicates the axis is a rotation axis.

 $\label{eq:table_interpolation} TABLE~I\\$  SCARA robotic arm URDF size parameter list

Joint	X (mm)	Y (mm)	Z (mm)	Rx	Ry	Rz
J1	0	0	0	0	0	1
J2	0	0	198.5	0	0	1
J3	600	0	18.5	0	0	1

The center of mass represents the point at which the entire mass of the robot is concentrated, and its position affects the robot's stability, balance, and overall dynamics. In a URDF model, the center of mass position is used to calculate various physical properties, such as the robot's moments of inertia, gravitational forces, and accelerations. It also plays a vital role in simulating and controlling the robot's movements. The center of mass parameter table for the URDF model in the SCARA robot is shown in Table 2. Where M is the mass, and Mx, My, and Mz are the position of the center of mass.

TABLE II
URDF CENTER OF MASS PARAMETER TABLE

UKD	URDF CENTER OF MASS PARAMETER TABLE					
Joint	M	Mx	My	Mz		
Joint	(KG)	(mm)	(mm)	(mm)		
J1	0	0	0	0		
J1 J2	0 19.57	0 350.8	0 0.006	0 10.241		

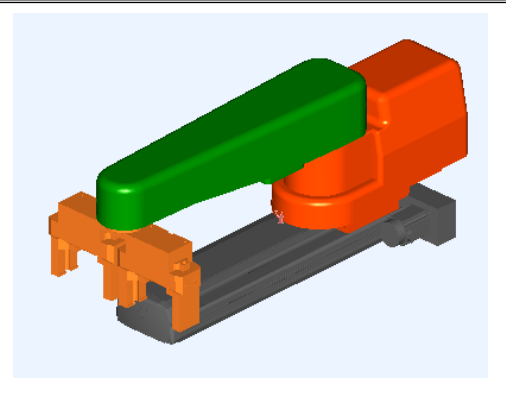


Fig. 2. SCARA robotic arm for the simulation program.

#### III. FUNDAMENTALS OF ROBOT DYNAMICS

This section briefly introduces the robot dynamics that will be used in the SCARA robot.

#### A. Robot Dynamics

In this research, a SCARA robotic arm is used for performing the control and modeling of the industrial collaborative robot. Joint 2 and joint 3 were targeted to demonstrate the effectiveness of their proposed approach, which could potentially be expanded to include other joints of the robot.

#### 1) Dynamics Modelling

For the N degree of freedom (DoF) robot manipulator, the dynamic model is formulated as follows:

$$M(q)\ddot{q} + C(q,\dot{q})\dot{q} + G(q) + \tau_f(q,\dot{q}) = \tau_m - \tau_{ext}$$
 (1)

where  $M(q) \in \mathbb{R}^{N \times N}$  denotes the mass matrix, which is a positive definite and symmetric matrix,  $C(q, \dot{q}) \in \mathbb{R}^{N \times N}$  denotes the centrifugal and the Coriolis effects,  $G(q) \in \mathbb{R}^N$  denotes the gravity term,  $\tau_f(q, \dot{q})$  denotes the friction torques of the robot joints,  $\tau_{ext} \in \mathbb{R}^N$  is the disturbance torque produced by an unknown environment with the robot manipulator, and  $\tau_m \in \mathbb{R}^N$  is the joint torque driven by servo motors

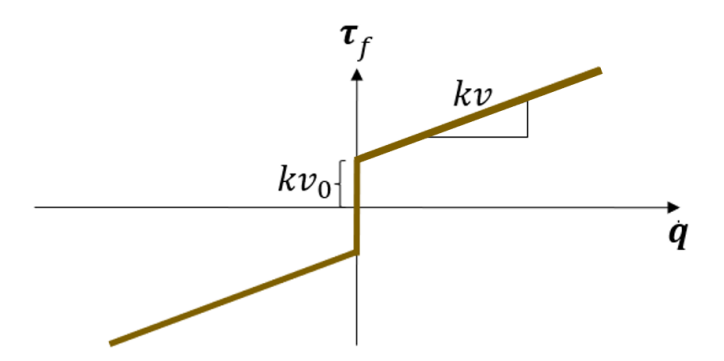


Fig. 3. Friction torque model for the manipulator.

#### 2) Friction Model

In dynamic mode, the friction generated between two surfaces in contact is not linear and is dependent on the relative velocity between them. The Stribeck model is commonly employed to describe this nonlinearity in friction. The Stribeck model can be utilized to determine the frictional behavior of a robot joint operating in dynamic mode. The Stribeck model is formulated as follows:

$$F(v) = F_{\rm C} + (F_{\rm S} - F_{\rm C}) \exp^{-|v/v_{\rm S}|^{\delta \rm S}} + F_{\rm v} v$$
 (2)

where  $F_{\rm C}$  denotes the Coulomb friction,  $F_{\rm S}$  denotes the static friction,  $v_{\rm S}$  denotes the Stribeck velocity, v denotes the joint velocity,  $\delta {\rm S}$  is the exponent of the Stribeck nonlinearity, and  $F_{\rm v}$  denotes viscous friction. In this study, joint 2 and joint 3 are tested independently.

First, the Stribeck parameters of the friction model in equation (2) are initially calibrated. A single joint undergoes movement at a constant speed. This motion is controlled by a joint torque resulting solely from gravity and friction torque, and there are no centrifugal or Coriolis forces involved in this scenario [12]. The dynamic model can be simplified to calculate the joint friction. When the joint moves clockwise and other joints are kept not moving, the torque of that joint is:

$$\boldsymbol{\tau}^{+} = \boldsymbol{G}(\tilde{\boldsymbol{q}}) + \boldsymbol{\tau}_{f}(\dot{\tilde{\boldsymbol{q}}}_{+}) \tag{3}$$

where  $\tau^+$  is the torque for a single joint moving clockwise with  $\tilde{q}$  denotes the joint position, and  $\dot{\tilde{q}}$  is the constant joint velocity. Meanwhile, for counterclockwise movement, the dynamics model is:

$$\boldsymbol{\tau}^{-} = \boldsymbol{G}(\tilde{\boldsymbol{q}}) + \boldsymbol{\tau}_{f}(\dot{\tilde{\boldsymbol{q}}}_{-}) \tag{4}$$

From (3) and (4), it can be derived that the friction robot torque can be calculated as:

$$\tau_f(\dot{\tilde{q}}) = \frac{(\tau^+ - \tau^-)}{2} \tag{5}$$

For mechanisms such as machine tools and manipulators with lubricated bearings as the core, the friction torque model is represented in the graph shown in Fig. 3, with the calculation formula:

$$\boldsymbol{\tau}_f(\dot{\tilde{\boldsymbol{q}}}) = k\boldsymbol{v} \times \dot{\tilde{\boldsymbol{q}}} + k\boldsymbol{v}_0 \tag{6}$$

where kv and  $kv_0$  are the adjustment parameter for kinetic friction coefficient and static friction coefficient.

## 3) Moment of Inertia

One method to calculate the moment of inertia of the second joint and the third joint of the SCARA robot is by assuming the link is a rectangular cuboid object. The moment of inertia is calculated with the formula:

$$I = m\frac{W^2 + L^2}{12} + mD^2 \tag{7}$$

where m is the mass of the object, D indicates the distance between the rotation axis and the center of gravity, W and L are the width and length of the object respectively, as shown in Fig. 4.

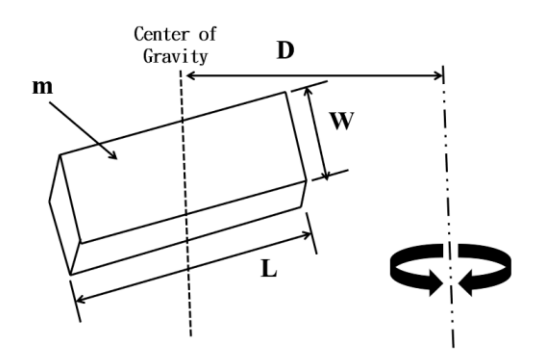


Fig. 4. Calculation of the moment of inertia of a rectangular cuboid object

Using CAD software to calculate the moment of inertia has several advantages over the manual calculation method. CAD software allows for more accurate measurements of complex shapes, which can be difficult to achieve using manual methods. This results in a more precise moment of inertia calculation, providing more accurate physical modeling of the object's behavior.

This project utilized Solidwork 3D model properties to calculate the moment of inertia. The 3D Solidwork model for the second and the third joint are shown in Fig. 5. The moment of inertia of the respective joint are shown in Table 3. The moment inertia with respect to the Z-axis is chosen since the Z-axis is the rotation axis.

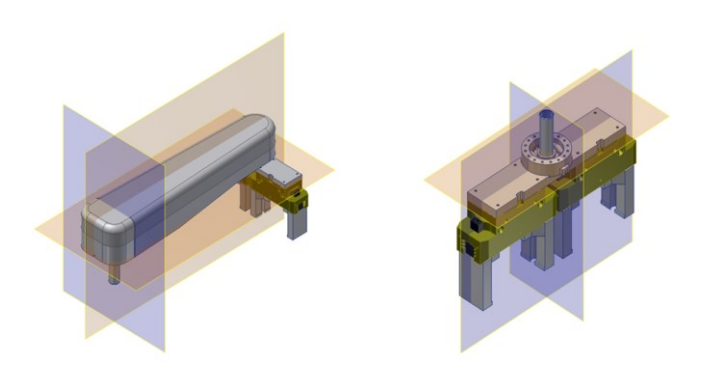


Fig. 5. Solidwork 3D model of the second and the third joint

TABLE III URDF ce<u>nter of mass paramet</u>er table

Joint	$I_{zz}  (kg \cdot m^2)$
J2	5.13445
J3	2.82815

# IV. CONTROL SCHEME AND POWER-ASSISTED COLLISION DETECTION STRATEGY

### A. Control Scheme

In this research, we directly modify the controller without the need for an additional force sensor. In order to make the robot arm a flexible robot arm, we limit the output of the controller through the torque switch and calculate the power assist compensation with the algorithm to achieve the function. Traditionally, the controller is controlled according to the target and the current state.

Fig. 6. Basic control diagram of the robotic arm.

As shown in Fig. 6, the typical control diagram for the arm robot consists of several parts. The command reference is the position; the feedback is the position feedback; the error is the position error, and the driver sends out the control output according to the position error. The stronger the external interference, the greater the position error will be, and the controller must generate greater control output to suppress the external interference.

For the power-assisted collision detection strategy, the socalled external disturbance is divided into two parts, the known load, and the unknown disturbance. The known load is the type of load that can be calculated in advance, such as inertial force and friction. The unknown disturbance is the type of load that cannot be calculated in advance that can be resulted from uncertain factors in the environment, such as collision.

To compensate for unknown disturbances, it is necessary to employ a traditional closed-loop control system in the driver. The motion of the robot can be utilized to calculate an extra torque to counteract these disturbances.

#### B. Power-assisted Collision Detection Strategy

Through the modeling methods proposed in the robot dynamics section, the sensorless power-assisted collision detection strategy can be achieved, including the application of the manual teaching mode of the robotic arm, the safety collision protection mode, and the flexible mode.

#### 1) Manual Teaching Mode

When the SCARA robotic arm enters the manual teaching mode, the control power limit is reduced to 0% so that the output of the controller is zero, and it can be pushed freely by hand. This enables the user to directly complete the task by moving the object manually by hand, as shown in Fig 7. The compensation value of each axis can also be fine-tuned to improve the operability of different users when using the manual teaching function.



Fig. 7. Manual Teaching Mode for the 2<sup>nd</sup> joint.

#### 2) Safety Collision Protection Mode

As shown in Fig. 8, the concept of the safety collision protection function is to compare the torque value calculated by

the combination of friction and inertia with the actual torque value. The collision stop mechanism is triggered when the actual torque value is bigger than 115% of the calculated value and 0.1 seconds has elapsed. It is determined that a collision has occurred, and the movement of the robot will be restricted by limiting the control power limit to 0%, or in other words, it enters the manual teaching mode.

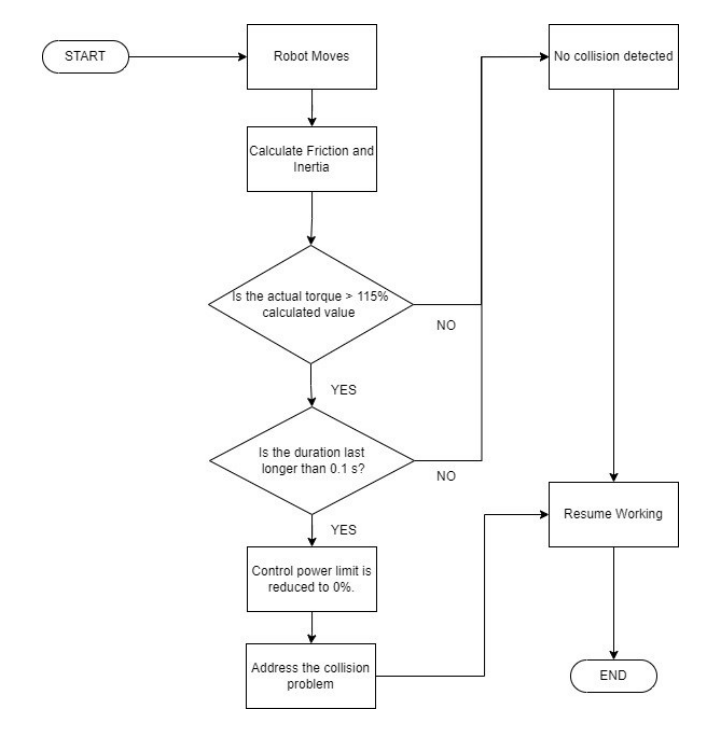


Fig. 8. Power-assisted control strategy for collision detection.

#### 3) Flexible Mode

This flexible operation mode is set by limiting the torque switch to 30%. It means that the closed-loop control force in the motor output is only 30% of its maximum power. In terms of physical quantity, it means that the 100W motor has only 30W controller output.

In the experiment, the hand is used to block the movement of the robot, and the torque value is limited by the value of the torque limiter. When the robot arm collides, it is less likely to cause damage to the robot arm because the torque limit is low.

#### V.EXPERIMENTS AND RESULT

# A. Friction Torque Calculation

As discussed in sections III and IV, the computed torque from motion control is calculated first. Then the value will be compared to the actual torque value for the power-assisted control strategy. For the friction calculation, the 2<sup>nd</sup> and the 3<sup>rd</sup> joint are tested with various speeds in the clockwise and counterclockwise directions, as shown in Table IV and V.

CAI	CULATED FRICT	TION TORQUE VALUE FOR	ORQUE VALUE FOR 2 <sup>ND</sup> JOINT		
G 1	Clockwise	Counterclockwise	Average		
Speed	$(\tau^-)$	$( au^+)$	$( au_f)$		
30	-34.30	32.9585	33.6304		
60	-44.51	43.8723	44.1949		
90	-50.70	50.7045	50.7057		
120	-55.28	55.4289	55.3549		
150	-58.39	58.3891	58.3908		

 $\label{eq:table v} TABLE\ V$  Calculated Friction Torque Value for  $3^{\text{RD}}$  Joint

Speed	Clockwise $(\tau^-)$	Counterclockwise $(\tau^+)$	Average $(\pmb{ au}_f)$
30	-25.0592	25.0879	25.0735
60	-33.3561	33.7424	33.5492
90	-38.6027	38.8647	38.7337
120	-42.5910	43.2197	42.9053
150	-45.5588	46.7232	46.1410

The speed of each joint can be mapped to friction torque value by utilizing a linear regression. The linear regression graph for the second and the third joint are shown in Fig. 9 and 10. Then according to (6), we can get the value for kv and  $kv_0$  as shown in Table VI. With those parameters, we can calculate the friction torque estimation for any speed. As previously mentioned, the percentage on the torque value indicates that the closed-loop control force in the motor output is limited to a specific percentage of its maximum power.

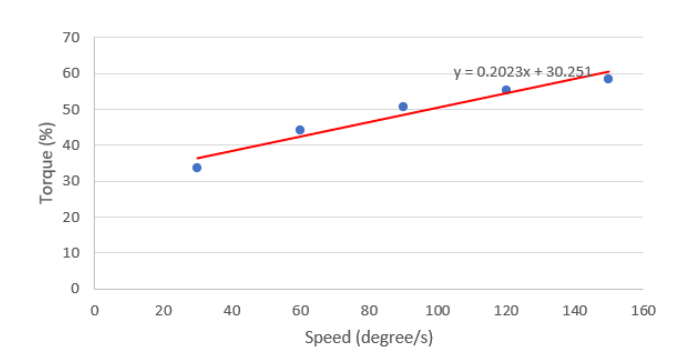


Fig. 9. Friction torque regression for the 2<sup>nd</sup> joint

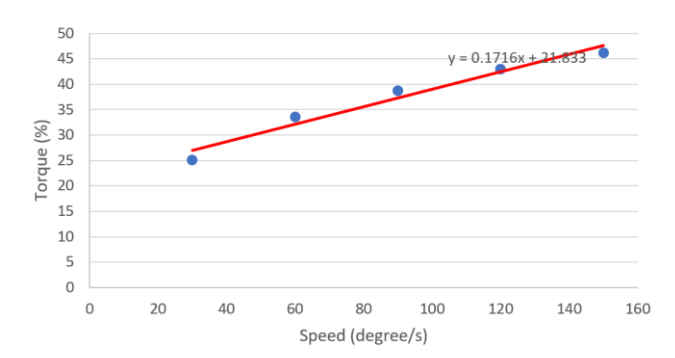


Fig. 10. Friction torque regression for the 3<sup>rd</sup> joint

kv and	$kv_0$	VALUE FOR	FRICTION	VALUE PARA	METER

Joint	kv	$kv_0$
J2	0.2023	30.251
J3	0.1716	21.833

#### B. Power-assisted Control Test

To test the effectiveness of the power-assisted control, the second and third joints are inspected. During the inspection, an operator holds the movement of the link by placing their hand in its trajectory while it is moving. This procedure is illustrated in Fig. 11.



Fig. 11. Collision test on 2<sup>nd</sup> joint.

Fig. 12 shows the time data series when the second joint is moving. At t=2.5 seconds, there is a big disparity between the estimated torque and the actual torque. This moment indicates that there is a collision detected, and the manual teaching mode will be executed. The same procedure is also tested for the third joint. As we can see from the graph in Fig. 13, there is a collision detected at t=2.7 seconds.

This collision detection will deploy a manual teaching mode so that the operator can configure or solve the problem that causes the abnormal status. After that, the robot resumes its original work target, enhancing the overall efficiency of the collaborative process.

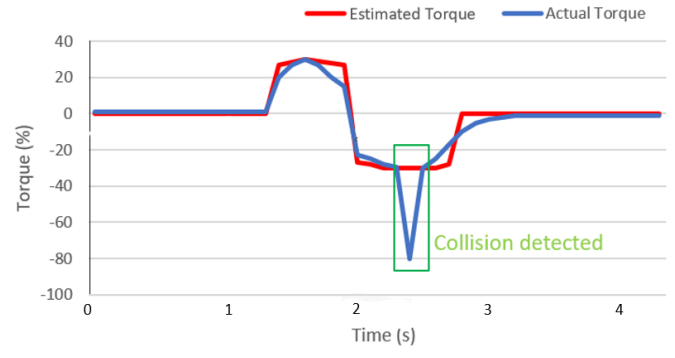


Fig. 12. Collision detection on t = 2.5 in  $2^{nd}$  joint

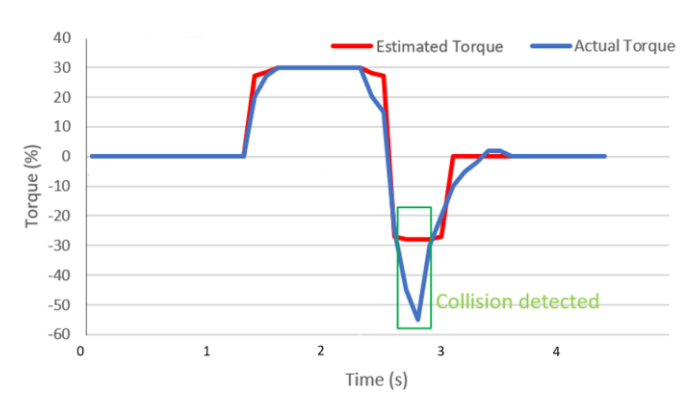


Fig. 13. Collision detection on t = 2.7 in  $3^{rd}$  joint

#### VI. CONCLUSION

This study presents a power-assisted collision detection strategy that is integrated into the controller, thus removing the requirement for an external force sensor. By utilizing the controller's mathematical model calculations and the driver's torque limit function, a force-limited robot that does not rely on additional sensors can be created. The mathematical model calculation module estimates the SCARA robot's friction and inertial force as compensation for the disturbance. With the calculated estimated torque, the power-assisted collision detection strategy can be deployed to enhance the collaborative function of the robot.

#### REFERENCES

- S. Haddadin, A. Albu-Schaffer, A. D. Luca and G. Hirzinger, "Collision Detection and Reaction: A Contribution to Safe Physical Human-Robot Interaction," in *IEEE/RSJ International Conference on Intelligent Robots and System*, Nice, France, 2008.
- [2] Y. Wu, P. Balatti, M. Lorenzini, F. Zhao, W. Kim and A. Ajoudani, "A Teleoperation Interface for Loco-Manipulation Control of Mobile Collaborative Robotic Assistant," *IEEE Robotics and Automation Letters*, vol. 4, pp. 3593 - 3600, 2019.
- [3] Q. Gao, J. Liu, Z. Ju and X. Zhang, "Dual-Hand Detection for Human-Robot Interaction by a Parallel Network Based on Hand Detection and Body Pose Estimation," *IEEE Transactions on Industrial Electronics*, vol. 66, no. 12, pp. 9663 9672, 2019.
- [4] R. K. Megalingam, R. S. Reddy, Y. Jahnavi and M. Motheram, "ROS Based Control of Robot Using Voice Recognition," in 2019 Third International Conference on Inventive Systems and Control (ICISC), Coimbatore, India, 2019.
- [5] P. Jaroonsorn, P. Neranon, C. Dechwayukul and P. Smithmaitrie, "Performance Comparison of Compliance Control based on PI and FLC for safe Human-robot Cooperative Object Carrying," in First International Symposium on Instrumentation, Control, Artificial Intelligence, and Robotics (ICA-SYMP), Bangkok, Thailand, 2019.
- [6] G. Gorjup, G. Gao, A. Dwivedi and M. Liarokapis, "A Flexible Robotic Assembly System Combining CAD Based Localization, Compliance Control, and a Multi-Modal Gripper," *IEEE Robotics and Automation Letters*, vol. 6, no. 4, pp. 8639 - 8646, 2021.
- [7] Y. Dong, T. Ren, D. Wu and K. Chen, "Compliance Control for Robot Manipulation in Contact with a Varied Environment Based on a New Joint Torque Controller," *Journal of Intelligent & Robotic Systems*, vol. 99, p. 79–90, 2020.
- [8] F. Mou, D. Wu and Y. Dong, "Disturbance rejection sliding mode control for robots and learning design," *Intelligent Service Robotics*, vol. 14, 2021.
- [9] F. Lange, C. Jehle, M. Suppa and G. Hirzinger, "Revised Force Control Using a Compliant Sensor with a Position Controlled Robot," in *IEEE*

- International Conference on Robotics and Automation, Minnesota, USA, 2012
- [10] I.-M. Kim, H.-S. Kim and J.-B. Song, "Design of joint torque sensor and joint structure of a robot arm to minimize crosstalk and torque ripple," in 9th International Conference on Ubiquitous Robots and Ambient Intelligence (URAI), Daejeon, Korea (South), 2012.
- [11] H. Zhang, W. Qin, Y. Gao, Q. Li, Z. Chen and J. Zhao, "Disturbance Elimination for the Modular Joint Torque Sensor of a Collaborative Robot," *Mathematical Problems in Engineering*, vol. 2020, 2020.
- [12] S. Liu, L. Wang and X. V. Wang, "Sensorless haptic control for humanrobot collaborative assembly," CIRP Journal of Manufacturing Science and Technology, vol. 32, pp. 132-144, 2021.



Isak Martin Simbolon, received his bachelor degree at Electrical Engineering Universitas Indonesia in 2019 majoring in Control Engineering. He received his M.Sc. degree in Departments of Electrical Engineering from National Taiwan University of Science and Technology, Taiwan, in 2022. He is currently a robotics engineer with the Precision Machinery Research & Development Center, Taichung City, Taiwan. His research interests and publications are in the robotics, machine learning, and computer vision.



Yun-Yu Yang, received the M.S. degree in Departments of Mechanical Engineering from National Chung Hsing University, in 2012. She is currently a robotics Engineer with the Precision Machinery Research Development Center. Her research interests and publications are in robotics, including controller programs and related algorithm development.